PHYSICAL REVIEW B **77**, 224113 (2008)

Atomistic simulations of the mechanical properties of silicon carbide nanowires

Zhiguo Wang,[1,*] Xiaotao Zu,[1] Fei Gao,[2] and William J. Weber[2]
[1]*Department of Applied Physics, University of Electronic Science and Technology of China,*
Chengdu, 610054, People's Republic of China
[2]*Pacific Northwest National Laboratory, P.O. Box 999, Richland, Washington 99352, USA*

(Received 15 May 2008; revised manuscript received 28 May 2008; published 25 June 2008)

Molecular-dynamics methods using the Tersoff bond-order potential are performed to study the nanomechanical behavior of [111]-oriented β-SiC nanowires under tension, compression, torsion, combined tension-torsion, and combined compression-torsion. Under axial tensile strain, the bonds of the nanowires are just stretched before the failure of nanowires by bond breakage. The failure behavior is found to depend on size and temperatures. Under axial compressive strain, the collapse of the SiC nanowires by yielding or column buckling mode depends on the length and diameters of the nanowires, and the latter is consistent with the analysis of equivalent continuum structures using Euler buckling theory. The nanowires collapse through a phase transformation—from crystal to amorphous structure—in several atomic layers under torsion strain. Under combined loading the failure and buckling modes are not affected by the torsion with a small torsion rate, but the critical stress decreases by increasing the torsion rate. Torsion buckling occurs before the failure and buckling with a big torsion rate. Plastic deformation appears in the buckling zone by further increasing the combined loading.

DOI: 10.1103/PhysRevB.77.224113 PACS number(s): 65.80.+n, 02.70.Ns

I. INTRODUCTION

Silicon carbide (SiC), one of the third-generation wide-band-gap semiconductor materials, is usually used in electronic devices under harsh environments due to its high strength, high breakdown electronic field, high thermal conductivity, high saturation drift velocity, and excellent physical and chemical stability.[1] One dimensional nanostructures of SiC have also attracted considerable attention for their unique physical and electronic properties due to quantum-size effects, making them to be important materials in nanotechnology and nanoscale engineering.[2,3] With the recent advances in crystal grown technology, SiC nanowires have been fabricated[4–9] as building blocks in the miniaturization of electronic devices. Most SiC nanowires are of cubic zinc-blend structure (β-SiC) growth along the [111] direction,[4–9] exhibiting mechanical properties superior to other forms of SiC. Wong *et al.*[10] measured the strength of SiC nanowires using atomic force microscopy combined with the lithography technique. The reported elastic modulus and the largest ultimate bending strength are 610–660 and 53.4 GPa, respectively, which are two or more times higher than the values measured previously for SiC whiskers with micrometer diameters.[11] As a compound semiconductor, SiC nanowires are expected to have outstanding thermal and mechanical strengths and can be used in the fabrication of nanodevices operating at high temperature. Understanding the mechanical behavior of SiC nanowires is essential and of significant importance in order to determine the strength of these materials for practical application as electronic or optical interconnects and as components in microelectromechanics. Molecular-dynamics (MD) simulations can provide new insights into nanowires' mechanical behavior and deformation mechanisms, and these methods have been widely used to study the nanomechanical behavior of various nanowires, such as metal nanowires,[12–15] intermetallic nanowires,[16] and semiconductor nanowires.[17–19] In this paper, we report the results of MD simulations on the nanomechanical behavior of [111]-oriented SiC nanowires.

II. SIMULATION METHODS

The atomic interactions are described by the Tersoff bond-order potential,[20,21] where the short-range interactions have been modified to match *ab initio* calculations[22] as described by Devannathem *et al.*[23] The modified potential has been used to study the melting temperature of β-SiC (Ref. 24) using a "semiconstant volume simulations."[25] The estimated melting temperature is 3050 K, which is in reasonable agreement with the reported experimental value of 2800 K and recent MD simulation result of 3250 ± 50 K.[26] The potential has been known to describe adequately the crystalline and amorphous phases of SiC and its nonstoichiometric alloys[27] and has been employed to study the ion irradiation induced defects,[28–30] thermal properties,[31,32] and surface reconstruction[33] of SiC. All of these results have demonstrated that the Tersoff potential is capable of describing the equilibrium and deformed structures of crystalline SiC nanowires. In order to make it properly describe the properties under large strains, Tang *et al.*[32,34] modified the potential using variable cutoffs to study elastic and thermal properties of SiC and brittle fracture of cubic SiC under hydrostatic pressure. We tested several cases using the same technique and found no difference by using the potential without adjusting the cutoffs. Although the first-principles quantum-mechanical methods generally give the most accurate results, they cannot be applied to a larger system and longer simulation time. The short-range potentials employed should not affect the main conclusions obtained in the present investigations and could provide some useful results.

MD simulations were performed on the [111]-oriented SiC nanowires. The nanowires with hexagonal, rectangular,

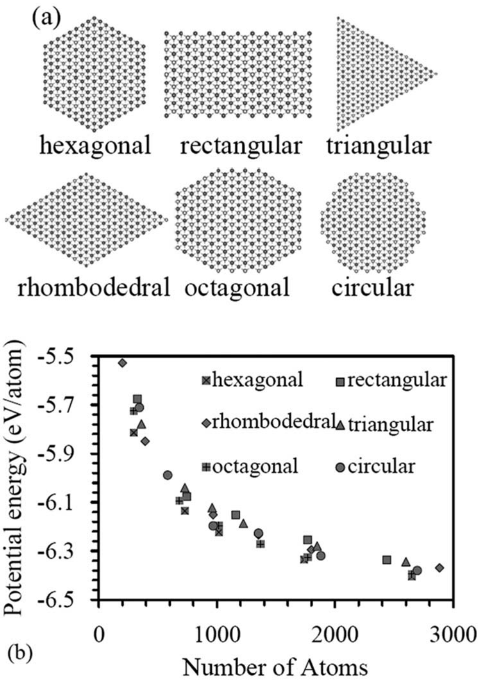

FIG. 1. (a) Cross-sectional shapes of SiC nanowires used in this work to examine the stability of nanowires; (b) Potential energies of the nanowires with various cross-sectional shapes calculated at 0 K. It is clear that the energy decrease as the number of atoms increases and that for a give shape.

triangular, rhombohedral, octagonal, and circular cross-sectional shapes are shown in Fig. 1(a) with different diameters, but all have a supercell length of 3.02 nm. These nanowires were used to examine their relative stabilities with different cross sections. It should be noted that the circular cross section is not perfectly circular, but its vertical and horizontal diameters are nearly equal and its shape closely resembles a circle. On minimizing the energy, the shapes of the nanowires did not change significantly. Figure 1(b) shows the potential energies of the nanowires with various cross-sectional shapes calculated at 0 K. It is clear that the energy decreases as the number of atoms increases for a given shape. This is because the larger diameter nanowires are less strained. A comparison of the different shaped nanowires with the same size shows that the nanowires with a hexagonal cross-sectional shape have the minimum potential energy, indicating that these nanowires are the most stable. These results agree with experimental results that demonstrate the most stable and natural cross-sectional configurations.[9,35] So nanowires with a hexagonal cross-sectional shape are used in this work. The computational models of SiC nanowires were constructed from the crystal structure of β-SiC along the [111] direction, with diameters ranging from 1.65 to 3.31 nm (the corresponding atom numbers change from 2184 to 7944). The diameter of the nanowires with a hexagonal cross section is defined as an average of two radial dimensions: center to corner and center to edge distances. A rigid boundary condition along the axial direction is used in this work. The initial structures of the nanowires are equilibrated for 100 ps at a given temperature, which allows the nanowires to reach stable configurations.

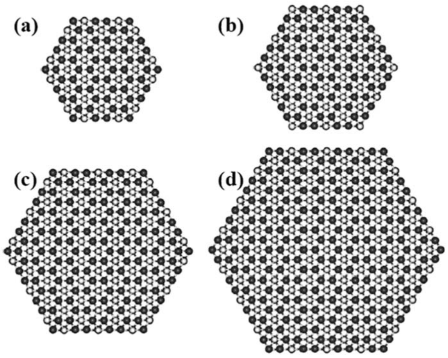

FIG. 2. Cross-sectional views of the [111]-oriented SiC nanowires. The nanowires diameters are (a) 1.65 nm, (b) 2.00 nm, (c) 2.64 nm, and (d) 3.31 nm.

III. RESULTS AND DISCUSSIONS

A. Relaxed SiC nanowires

Figure 2 shows the top views of the geometry of the four simulated SiC nanowires. The relaxed configurations show that the surface layer atoms undergo a bond-length contraction in which the C surface atoms only relax parallel to the surface, while the Si surface atoms relax parallel and perpendicular to the surface, moving radially inward by 0.012 nm. The relaxation of the atoms on the second outmost layers is very small. The relaxed SiC bond length on the outmost surface layer is 0.186 nm, which contracts by 1.58% compared with that in the bulk SiC. The ripple surface structure obtained in this work is in agreement with other theoretical predictions.[36,37]

B. Tensile behavior

The tension or compression was performed by displacing the top and bottom fixed five atomic layers in opposite directions at a constant strain rate, and the remaining atoms in the middle part are free to relax in time. The simulation strain rates of 0.003% ps^{-1} ~0.3 m/s were used in this work. In the present simulations, the time step was set to be 0.5 fs. The axial stress was taken as the arithmetic mean of the local stresses over all the atoms and was computed by averaging over the final 2000 relaxation steps during each strain increment. The length of 9.06 nm was used to investigate the tensile behavior.

Figure 3 shows the tensile stress-strain relationship for the tensile process of SiC nanowires with four different diameters at various temperatures. All the stress-strain curves are similar, irrespective of diameters and temperatures. The stress-strain curves show the same characters as those of the [100]-oriented SiC rod under tensile strain with an extension rate of 2 m/s,[27] which demonstrates the brittle failure. The stress increases with increasing strain of up to a threshold value that is defined as the critical stress for yield, but the further increase in strain leads to the abrupt dropping of stress. For example, for the nanowires with a diameter of 2.00 nm, the stress increases with increasing strain of up to 111 GPa (at strain of 27.3%) and 47.1 GPa (at strain of 14.6%) at 300 and 1800 K, respectively, and further in-

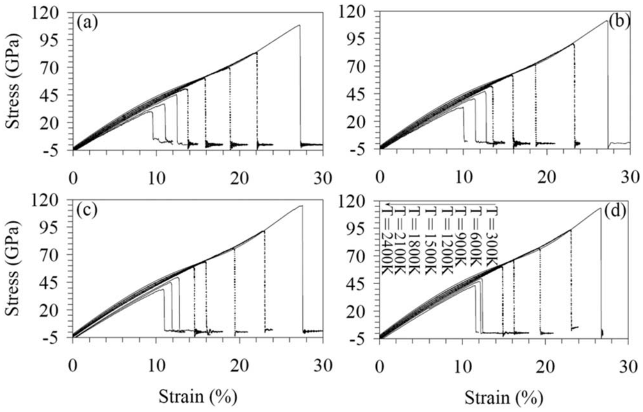

FIG. 3. Stress-strain curves for the tensile process of SiC nanowires at various temperatures with diameters of (a) 1.65 nm, (b) 2.00 nm, (c) 2.64 nm, and (d) 3.31 nm.

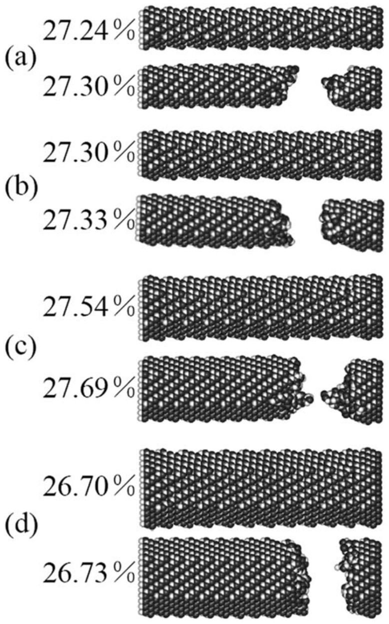

FIG. 4. Atomic configurations at several stages under tension at 300 K for the SiC nanowires with four different diameters of (a) 1.65 nm, (b) 2.00 nm, (c) 2.64 nm, and (d) 3.31 nm.

creases in strain and lead to stress abruptly decreasing to ~0.0 GPa. Judging from the character of the stress-strain dependences, we can assume that the SiC nanowires will fail without exhibiting any plasticlike behavior.

Young's moduli determined from the stress-strain curves with the strain $<3.0\%$ using linear regression are 520, 532, 546, and 555 GPa for the four nanowires with diameter in increasing order at 300 K. Young's modulus along the [111] direction obtained by Lambrecht *et al.*[38] is 603 GPa using the full potential linear muffin-tin orbital method, while it is 558 GPa calculated by Li *et al.*[39] using the pseudopotential plane-wave method. Petrovic *et al.*[40] measured Young's modulus of β-SiC whisker, with an average value of 581 GPa with $\pm 10\%$ scattering. Applying the equation of the cantilever beam, Wong *et al.*[10] measured Young's modulus of [111]-oriented SiC nanorod with a diameter of 21.5 nm is 660 GPa. So the computed values in the current simulations agree well with previous data. The computed Young's moduli for the four studied nanowires at various temperatures are summarized in Table I. Young's modulus depends on the nanowire size and simulation temperature and increases with the size of the system and decreases with temperature due to the softness of the nanowire materials.[41] Young's moduli of the nanowires are also larger than the corresponding values of a [100]-oriented SiC rod and bulk SiC,[27] indicating that SiC nanowires have great potential for use in composite materials as reinforcements.

The evolution of atomic configurations at several stages under tension at 300 and 1800 K for the SiC nanowires with four different diameters is shown in Figs. 4 and 5, respectively. Under the critical strain, the bonds of the nanowires are just stretched and preserve their fourfold coordination in the nanowires, and no structural defects appear at this stage. With further stretching, bond breakage in the outmost layer is observed and rapidly spreads toward the center as the strain increases. Several atomic chains can be seen before the nanowires rupture. When a single crystal is stretched, the fundamental deformation mechanism is a shearing action based on the resolved shear stress on an active slip system. The β-SiC is a diamond structure and its slip plane is {111},[42,43] whereas the load is along the [111] orientation in the present simulation, the resolved shear stress on the (111) plane is zero, which implies that no shearing takes place. The deformation will proceed by bond stretching and breakage without local necking.

Figure 6 shows the variation in the critical stress with temperature for the SiC nanowires. The results clearly show that the critical stress decreases with increasing temperature. Consequently, the mechanical properties of nanowires are sensitive to the temperature. At higher temperature, the atomic structure has high entropy, and the atoms vibrate about their equilibrium position at much larger amplitude, as compared to those at low temperatures. Thus, bond breakage becomes much easier at higher temperatures, which may

TABLE I. Young's modulus (in GPa) of the SiC nanowires with different diameters at temperatures of 300–2400 K obtained from stress-strain curves with the strain $<3.0\%$ using linear regression.

D (nm)	300 K	600 K	900 K	1200 K	1500 K	1800 K	2100 K	2400 K
1.65	520	508	496	484	473	471	452	448
2.00	532	520	510	497	487	483	479	454
2.64	546	535	523	512	500	493	492	474
3.31	555	544	533	521	512	504	504	483

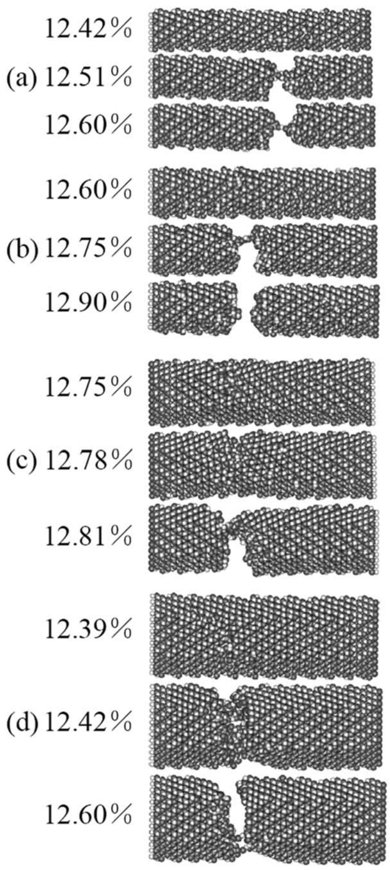

FIG. 5. Atomic configurations at several stages under tension at 1800 K for the SiC nanowires with diameters of (a) 1.65 nm, (b) 2.00 nm, (c) 2.64 nm, and (d) 3.31 nm.

suggest that a thermally activated process plays an activating role in the complete elongation of the SiC nanowires.

C. Compressive behavior

Figure 7 shows the compressive stress-strain relationship of the SiC nanowires with four different diameters and lengths at 300 K. The stress increases with the increase in strain and decreases after passing a threshold value. The atomic configurations show that short and long nanowires under compression exhibit different modes for the collapse of the SiC nanowires, one with yielding and another with column buckling, respectively. Figure 8 represents the compressive yielding process for the nanowires with a diameter of 2.00 nm at a length of 4.53 nm. It is clear that the SiC nanowires progressively shorten when compression increases but remain straight up to a strain of 13.89%; the nanowires deform by yielding with further increase of strain. For the longer nanowires with the same diameter, the failure of the nanowires changes to a buckling mode due to the instability of the structure. The critical buckling stress is much smaller than the compressive yielding stress. As the nanowires buckle, instead of remaining straight, they become curved. Figure 9 shows the buckling configurations for the nanowires with a diameter of 2.00 nm at a length of 12.08 nm.

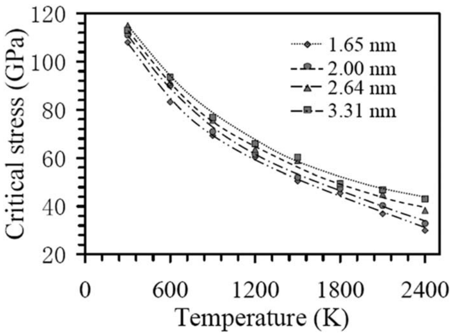

FIG. 6. Temperature dependence of the critical stress of the SiC nanowires. The critical stress decreases with temperature and increases with diameter.

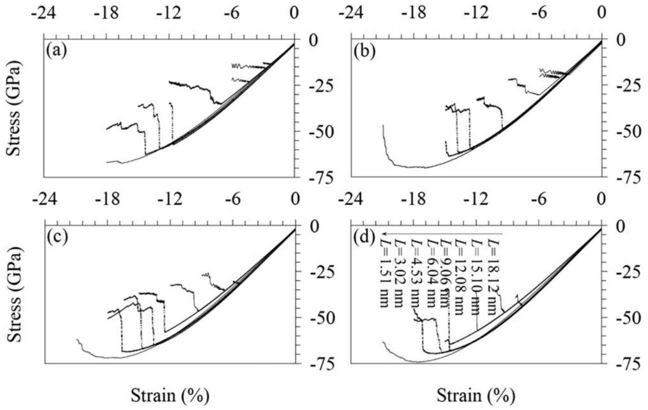

FIG. 7. Compressive stress-strain relationship of the SiC nanowires with different diameters and wire length, simulated at 300 K.

The critical compression strength obtained from the MD simulations is compared with the theoretical Euler buckling load. The latter is given by[44]

$$P_{cr}=\frac{\pi^2 EI}{L_e^2}, \tag{1}$$

where E is Young's modulus and L_e is the effective length of the tube. Both ends of the tubes are fixed against rotation so that $L_e=L/2$,[45] where L is the length of the tube, and I is the moment of inertia. The critical stresses at buckling versus the wire length obtained using MD simulation and Euler theories are shown in Fig. 10. As can be seen from the figure, the results of Euler column theory and MD simulations are very close to each other for wire lengths longer than 10 nm, the

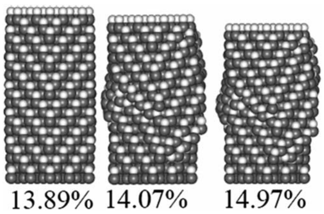

FIG. 8. Atomic configurations show the compressive yielding process for the nanowires with diameter of 2.00 nm at a length of 4.53 nm.

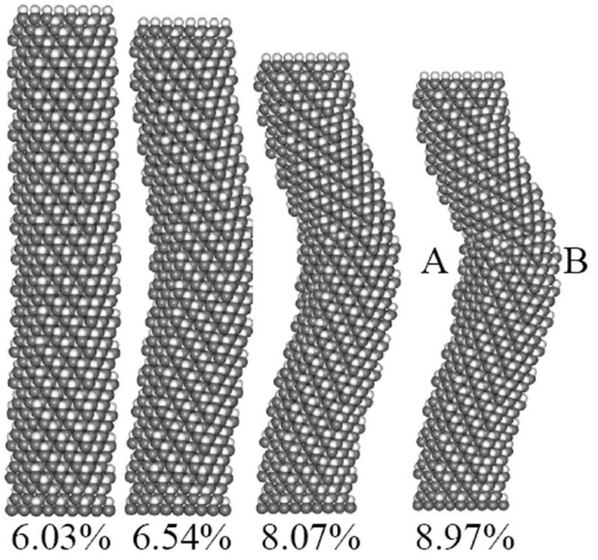

FIG. 9. Atomic configurations show the column buckling process for the nanowires with a diameter of 2.00 nm at a length of 12.08 nm.

critical stress decreases inversely with the square of the wire length for the nanowire with a diameter of 1.65 nm. However, for wire lengths shorter than 10 nm, the critical stress obtained from the MD is much smaller than that given by the Euler buckling theory, and the critical stress shows less dependence on the wire length. We should note that the Euler buckling theory only predicts the critical buckling stress for columnar buckling. Because the buckling mode shifts from a columnar mode to a yielding mode as the wire length decreases, the prediction of the critical stress given by MD simulation is much less than that given by the Euler buckling theory. From Fig. 10, it is also observed that the critical stress increases with increasing diameter of nanowires of the same length. The critical stress as a function of diameter of nanowires is shown in Fig. 11. We find that the theoretical critical compressive stress fits well to a linear dependence on the nanowire diameters D (nanometers) for wire lengths shorter than 6.04 nm and longer than 15.1 nm. However, for wire lengths in the range between 6.04 and 15.1 nm, the critical stress cannot be fitted linearly. The dependence of critical stress on the diameter at a length of 1.51 nm can be fitted by $P_{cr}=4.225D+60.51$, which may attribute to the different collapse modes. If the nanowires collapse with yielding or column buckling mode, the critical stress will increase linearly. However, as the wire length ranges from 6.04 to 15.1 nm with diameters of 1.65 and 2.00 nm, the nanowires collapse through column buckling, whereas the nanowires with diameters of 2.64 and 3.31 nm collapse through yielding mode. This may explain why the critical stress cannot be fitted into a linear relationship with the diameter in the present simulations.

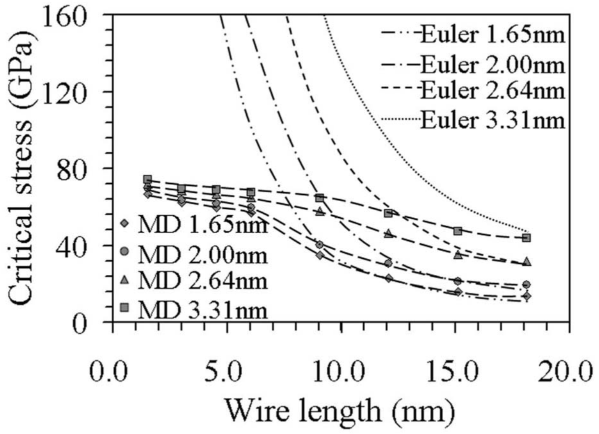

FIG. 10. The wire length dependence of the critical stresses obtained by MD simulations and Euler theory.

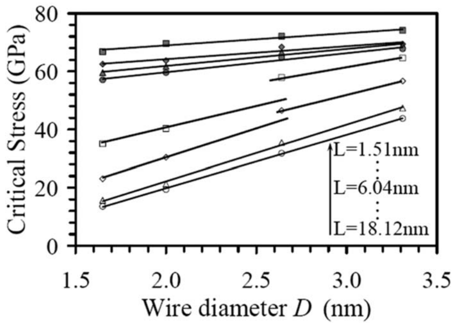

FIG. 11. Critical stress as a function of the nanowires diameter, which shows that critical buckling stress increases linearly with increasing diameter if the nanowires collapse in a similar mode for the same length.

D. Torsion behavior

The torsion was performed by keeping fixed one end of the nanowires, while the torsion loads are applied to another end, and the remaining atoms in the middle part are free to relax. A time step of 0.5 fs is used. The energy of the initial strain free configurations is denoted as E_0 and that of the strained system is denoted as E_l. The strain energy $E_s=E_l-E_0$ is accumulated in the nanowires due to torsion. Figures 12(a) and 12(b) show the strain energy as a function of torsion angle for the nanowires with a diameter of 2.0 nm and length ranged from 3.02 to 18.12 nm at 300 and 1500 K, respectively. The torsion rates of 0.01° and 0.15° ps^{-1} are used at 300 and 1500 K, respectively. As seen from Fig. 12, there is a critical value of torsional angle, beyond which plastic defects occur with a sudden drop in the accumulated torsional strain energy. This angle corresponds to the critical torque τ_c, below which the nanowires can sustain without any loss in structure integrity and the strain energy E_s increases with the increasing of torsional angle θ, following a quadratic form $E_s=k\theta^2$. The evolution of the atomic configuration of the nanowire with a diameter of 2.0 nm and a length of 12.08 nm under different torsion angles at a simulation temperature of 300 K is shown in Fig. 13. The whole structure retains hexagonal cross section as the torsion angle is smaller than 221°. The atoms move only along the circumferential direction and the crystal lattices preserve their original arrangements. Once the torsion angle exceeds the critical value, a slight collapse of the structure takes place in the

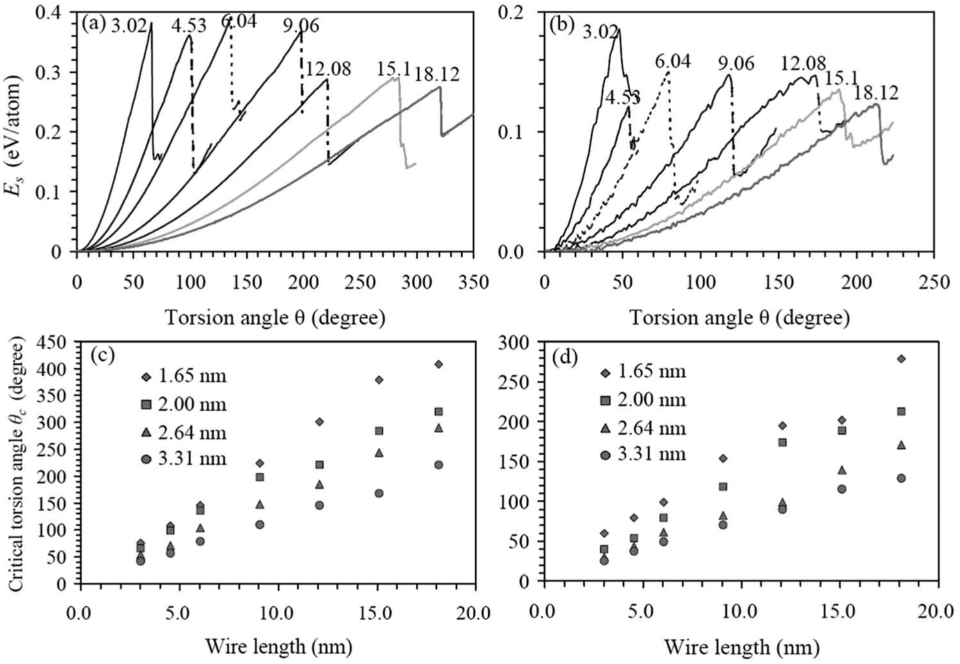

FIG. 12. Strain energy as a function of torsion angle for the nanowires with a diameter of 2.0 nm and length changed from 3.02 to 18.12 nm at (a) 300 K and (b) 1500 K. Critical torsional angles as a function of wire length at (c) 300 K and (d) 1500 K.

middle part of the nanowires. Crystal to amorphous structure transition can be observed in the collapse part. The configuration deforms more violently as the torsion angle increases.

The torsional buckling is also found to strongly depend on the length of the nanowire. The critical torsional angles as a function of wire length at 300 and 1500 K are shown in Figs. 12(c) and 12(d), respectively. It is clearly shown that the critical torsional angle increases with the increasing of wire length. Since the torsional buckling occurs as a result of dynamic processes, the mechanisms of material deformation can also be influenced by temperatures. Thus, the effect of temperature on the buckling behavior is also investigated. The critical torsional angle as a function of temperature is shown in Fig. 14 for the nanowires with a length of 9.06 nm. As can be seen from the figure, the critical torsional angles depend on the temperature and diameter of the nanowires. The critical torsional angle decreases with the increasing of temperature. This result suggests that a thermal activated process plays an activating role in the buckling of SiC nanowires. At higher temperatures, the atomic structure has higher entropy, and the atoms vibrate around their equilibrium positions at much larger amplitude, as compared to the low temperatures, and hence deformation occurs easily. The critical torsional angle also depends on the diameter of the nanowires, the larger critical angles correspond to thinner nanowires. This is probably due to the effect of increased surface-to-volume ratio, which allows for nonlinear relaxation of the accumulated stress in the most efficient way for atomically resolved model systems.

E. Combined tension-torsion

A fixed boundary condition is assumed at one end of the nanowire, while the combined tensile-torsion loads are applied to the another end. The applied strain is increased slightly to deform the SiC nanowires. The combined tension-torsion or compression-torsion is applied simultaneously during the simulations. In all the simulations, a time step of 0.5 fs is used. All the atoms are first allowed to move freely until the structure reaches the minimum-energy configuration at a given temperature, and then the combined tension-torsion loading is applied. The deformed nanowire is relaxed for 10

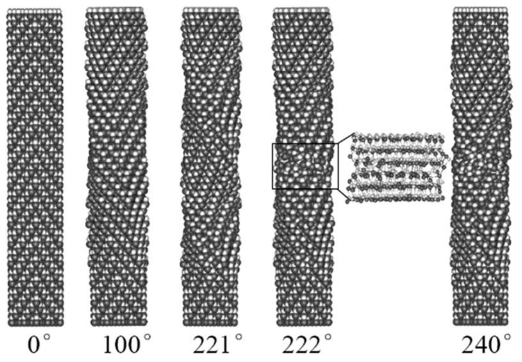

FIG. 13. Evolution of the atomic configuration of nanowires with a diameter of 2.0 nm and a length of 12.08 nm under different torsion angles at a simulation temperature of 300 K.

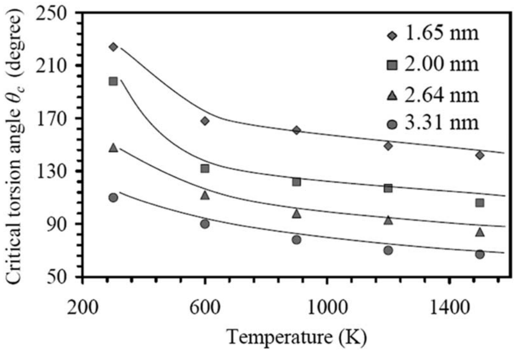

FIG. 14. Critical torsional angle as a function of temperature.

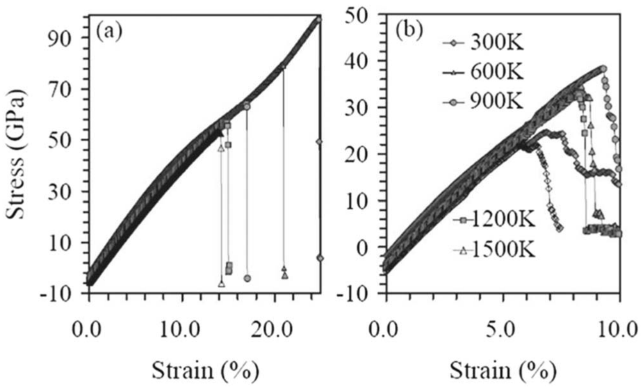

FIG. 15. Tensile stress-strain curves for (a) nanowires with a diameter of 2.0 nm and with a torsion strain rate of 0.02° ps^{-1} and (b) nanowires with a diameter of 3.31 nm and with a torsion strain rate of 0.10° ps^{-1} at various temperatures.

ps, and the relaxed structure is used as an initial configuration for the next MD step. The stress during each strain increment is computed by averaging over the final 2000 relaxation steps. A strain rate of 0.005% ps^{-1} is used in the tensile and compressive loading, and torsion rate changes from 0.02° to 0.15° ps^{-1}.

Figure 15(a) shows the relationships between tensile stress and strain for the nanowires with a diameter of 2.0 nm and with a torsion strain rate of 0.02° ps^{-1} at various temperatures. The stress-strain curves show the same characteristic as that of pure tension. The stress increases with increasing strain up to a maximum value but further increase in strain leads to the stress abruptly dropping to about 0 GPa. The evolution of atomic configurations before and after failure under tension at 300–1500 K is shown in Fig. 16. The nanowires deform through bond stretching and breakage under the combined tension-torsion with a torsion strain rate of 0.02° ps^{-1}. The relationships between tensile stress and strain for the nanowires with a diameter of 3.31 nm and with a torsion strain rate of 0.10° ps^{-1} at various temperatures are shown in Fig. 15(b). The stress-strain curves show the different characteristics as that of pure tension [as shown in Fig. 3(d)]. The stress decreases slowly with the increase of the strain after passing the critical stress. The evolutions of the atomic configurations at several stages under combined tension-torsion for the nanowires with a diameter of 3.31 nm and a torsion strain rate of 0.10° ps^{-1} at 300 and 1500 K are shown in Figs. 17(a) and 17(b), respectively. The whole structure retains hexagonal cross section as the tensile strain is smaller than 5.80% and 5.00% at 300 and 1500 K, respectively. The atoms move only along the circumferential direction and the crystal lattices preserve their original arrangements. As the strain increases further, a slight collapse of the structure takes place in the nanowires as circled by the dotted lines, and this part transforms to amorphous phase as with further increase in the strain. Plastic deformation appears in the amorphous zone with further increase in the strain. So the fracture behavior changes from a brittle manner to a ductile manner.

Figure 18 shows the critical tensile stress as a function of temperature. The critical stress decreases with the increase in temperature except for the nanowires with bigger diameters and with larger torsion rate, in which case the critical stress increases first with increasing temperature and then decreases. For example, the critical stress increases from 24.3 to 38.3 GPa as the temperature increases from 300 to 900 K for the nanowire with a diameter of 3.31 nm and a torsion rate of 0.10° ps^{-1}. With a low torsion rate the torsion buckling does not occur before tensile failure, the combined tension-torsion dose not change the failure mode of the nanowires. As discussed above, a thermal activated process plays

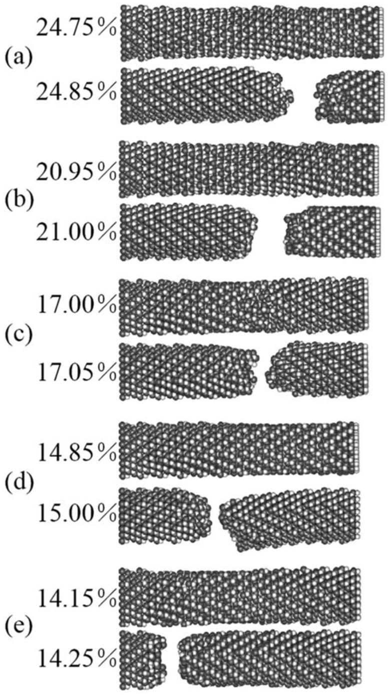

FIG. 16. The evolution of atomic configurations before and after failure under tension at 300–1500 K for the nanowire with a diameter of 2.00 nm; the torsion rate is 0.02° ps^{-1}.

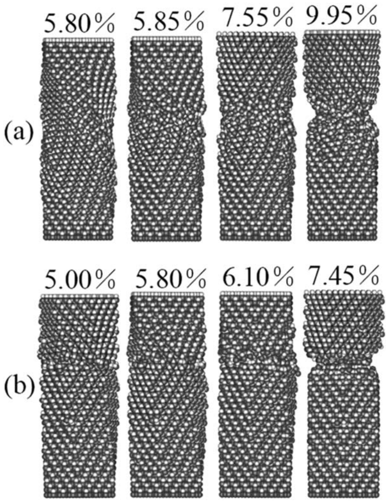

FIG. 17. The evolutions of the atomic configurations at several stages under combined tension-torsion for the nanowires with a diameter of 3.31 nm and with a torsion strain rate of 0.10° ps^{-1} at (a) 300 K and (b) 1500 K.

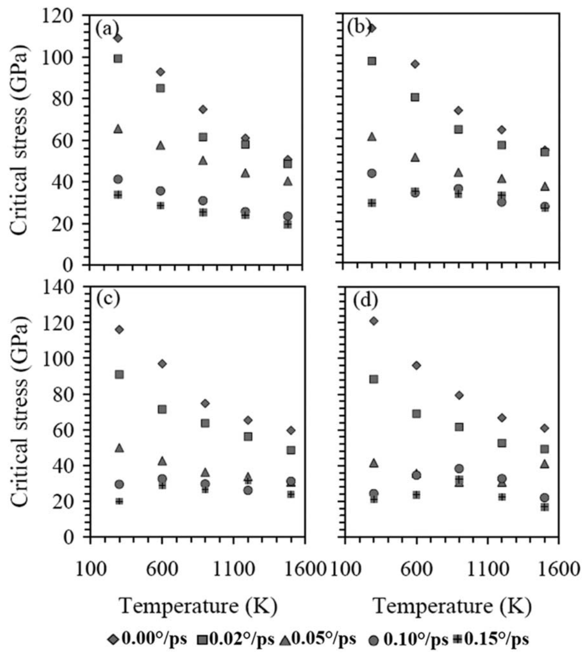

FIG. 18. Critical tensile stresses as a function of temperature for the nanowires under combined tension-torsion.

an activating role in the tensile failure of the SiC nanowires, and thus, the critical tensile stress decreases with increasing the temperature. Torsion deformation will lower the energy barrier for bond ruptures such that the critical stress decreases with increasing torsion rate. With large torsion rate, the torsion buckling occurs before the failure of the nanowires, and the plastic deformation primarily appears in the buckling zone under further combined loading. The critical stress shows a different dependence on the temperature as that with lower torsion rates.

F. Combined compression-torsion

Figures 19(a) and 19(b) show the stress-strain curves for the nanowire with a diameter of 2.00 nm at 300 and 1500 K, respectively, with torsion strain ranged from 0.00 to 0.15° ps^{-1}. The stress increases with increasing strain up to a maximum value but further increase in strain leads to dropping of the stress. It is clear that the linear part of the stress-strain curves completely overlap, which implies that the torsion rate has no significant effect on the elastic properties of SiC nanowires.

The buckling loads as a function of torsion rate for the nanowires under combined compression-torsion loading at 300 and 1500 K are shown in Figs. 19(c) and 19(d), respectively. The buckling load decreases with increasing torsion rate. For example, the critical stress decreases from 61.3 to 18.7 GPa as the torsion rate increases from 0.0 to 0.15° ps^{-1} for a nanowire with a diameter of 2.64 nm at 300 K. The larger torsion rate lowering the critical stress can be attributed to the fact that larger torsion lowers the energy barrier for the deformation of the nanowires.

Figure 20 shows the side views of the atomic configurations at different stages of the nanowires with a diameter of

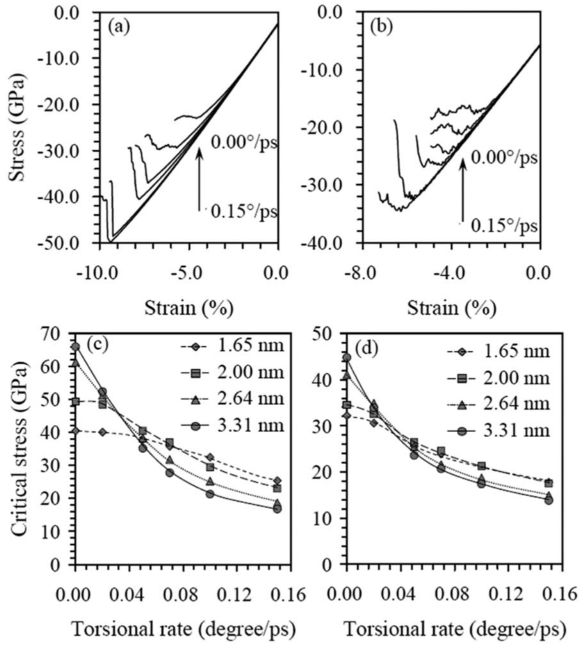

FIG. 19. Stress-strain curves for nanowire with a diameter of 2.00 nm at (a) 300 K and (b) 1500 K under combined tension-torsion with torsion strain changed from 0.00 to 0.15° ps^{-1}. The buckling load as a function of torsion rate for the nanowires under combined compression-torsion loading at (c) 300 K and (d) 1500 K.

2.00 nm and torsion rates of 0.02°, 0.07°, and 0.15° ps^{-1} at a simulation temperature of 300 K. With the rates of 0.02 and 0.07° ps^{-1} the torsion does not change the collapse mode of the nanowires, which still collapse with a column buckling mode. However, the nanowires collapse through atom rearrangement under combined compression-torsion with a torsion rate of 0.15° ps^{-1}. This is because the torsion buckling occurs before the compression buckling.

As the collapse mode of the SiC nanowires depends on the length and diameters of the nanowires, the response of the nanowires with different lengths under combined compression-torsion is investigated with a torsion rate of 0.05° ps^{-1}. The compressive stress as a function of strain for the nanowire with a diameter of 2.00 nm and length ranged from 3.02 to 18.12 nm at 300 and 1500 K are shown

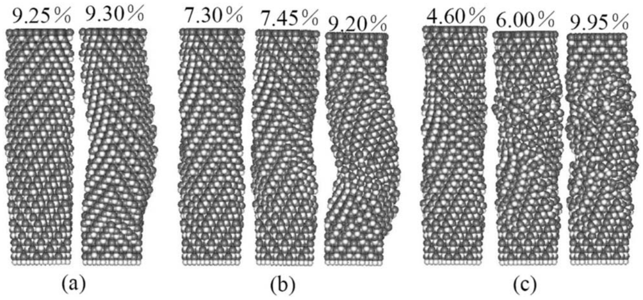

FIG. 20. Side views of the atomic configurations at different stages of the nanowires with a diameter of 2.00 nm under combined compression-torsion with torsion rates of (a) 0.02° ps^{-1}, (b) 0.07° ps^{-1}, and (c) 0.15° ps^{-1} at a simulation temperature of 300 K.

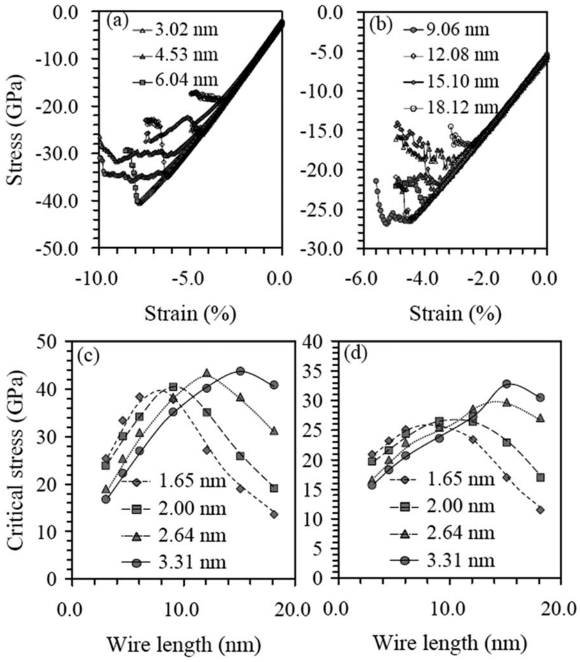

FIG. 21. Compressive stress as a function of strain for the nanowire with a diameter of 2.00 nm and length changed from 3.02 to 18.12 nm at (a) 300 K and (b) 1500 K. Dependence of critical buckling stress on the wire length under combined compression-torsion at (c) 300 K and (d) 1500 K.

in Figs. 21(a) and 21(b), respectively. As seen from the figures, the stress-strain relationship follows Hooke's law for low strains, the stress increases almost linearly with increasing strain up to a threshold value that is defined as the critical stress, and further increase in strain leads to decrease in stress. Figures 21(c) and 21(d) show the dependence of critical buckling stress on the wire length under combined compression-torsion at 300 and 1500 K, respectively. There is a critical length, below which the critical stress increases with increasing the length, but above which the critical stress decreases. The critical length increases with increasing the diameter of the nanowires, and they are ~6.04, ~9.06, ~12.08, and ~15.1 nm for the nanowires with diameters of 1.65, 2.00, 2.64, and 3.31 nm, respectively. Compared with the buckling critical stress under pure compression (Fig. 10), we notice that the critical stress decreases under the combined compression-torsion as the wire length is shorter than the critical length but shows almost no changes as the length is longer than the critical length. The atomic evolutions of the nanowires with a diameter of 2.64 nm and lengths of 4.53 and 15.1 nm are shown in Figs. 22(a) and 22(b), respectively, under combined compression-torsion. It is clearly shown that the combined compression-torsion does not alter the buckling mode of the long nanowires, and thus, the critical stress shows almost no changes as compared with buckling load of the nanowires with pure compressive strain. For the nanowires with a length of 4.53 nm, the atoms move only along the circumferential direction, and the crystal lattices preserve their original arrangements up to a compressive strain of 7.15%. As the strain reaches 7.8%, a small collapse of the structure takes place in the middle part of the nanowires. Crystal to amorphous (*c*-*a*) structure transition can be observed in the collapse part. The atomic configuration deforms more violently as the torsion angle increases, indicating that the short nanowires collapse through the *c*-*a* transition under combined compression-torsion. This induces the decrease in the critical buckling stress, as compared with that with pure compression.

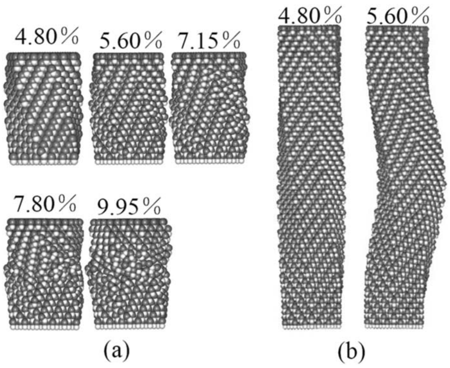

FIG. 22. Evolutions of atomic configurations of nanowires with a diameter of 2.64 nm and a length of (a) 4.53 and (b) 15.1 nm under combined compression-torsion.

IV. SUMMARY AND CONCLUSIONS

In summary, the nanomechanical behaviors of β-SiC nanowires with different diameters are investigated using molecular dynamics methods under uniaxial tensile and compressive loadings. The results show that the nanowires deform through bond-stretching and breaking in response to the axial tension. Young's moduli obtained from the stress-strain curves are 520, 532, 546, and 555 GPa for the four nanowires at 300 K and increases with diameter and decreases with temperature due to the softness of the nanowire materials. Under axial compressive strain, the collapse of SiC nanowires through yielding or column buckling mode depends on the length and diameter of the nanowires, and the latter is consistent with the prediction of equivalent continuum structures using Euler buckling theory. We also find that the critical buckling stress increases linearly with increasing diameter for a similar collapse mode at the same length. The nanowire collapse through a phase transformation from crystal to amorphous structure in several atomic layers under torsion strain. Under combined loading the failure and buckling mode are not affected by the torsion with a small torsion rate, but the critical stress decreases with increasing torsion rate. Torsion buckling occurs before the failure and buckling with a big torsion rate. Plastic deformation appears in the buckling zone with further increasing strain. The torsion rate has no effect on the elastic properties of SiC nanowires.

ACKNOWLEDGMENTS

Z.G.W. and X.T.Z. are grateful for the National Natural Science Foundation of China (Grant No. 10704014) and the Young Scientists Foundation of UESTC (Grant No. JX0731). F.G. and W.J.W. were supported by the Division of Materials Sciences and Engineering, Office of Basic Energy Sciences, U.S. Department of Energy under Contract DE-AC05-76RL01830.

---

*Corresponding author; zgwang@uestc.edu.cn

[1] *Properties of Silicon Carbide*, edited by G. L. Harris (INSPEC, Institution of Electrical Engineers, London, 1995).
[2] H. Seong, H. Choi, S. Lee, J. Lee, and D. Choi, Appl. Phys. Lett. **85**, 1256 (2004).
[3] B. H. Yan, G. Zhou, W. H. Duan, J. Wu, and B. L. Gu, Appl. Phys. Lett. **89**, 023104 (2006).
[4] X. H. Sun, C. P. Li, W. K. Wong, N. B. Wong, C. S. Lee, S. T. Lee, and B. K. Teo, J. Am. Chem. Soc. **124**, 14464 (2002).
[5] Y. Zhang, T. Ichihashi, E. Landree, F. Nihey, and S. Iijima, Science **285**, 1719 (1999).
[6] H. Dai, E. W. Wong, Y. Z. Lu, S. S. Fan, and C. M. Lieber, Nature (London) **375**, 769 (1995).
[7] G. Y. Yang, R. B. Wu, J. J. Chen, Y. Pan, R. Zhao, L. L. Wu, and J. Lin, Nanotechnology **18**, 155601 (2007).
[8] W. M. Zhou, X. Liu, and Y. F. Zhang, Appl. Phys. Lett. **89**, 223124 (2006).
[9] G. Z. Shen, Y. Bando, C. H. Ye, B. D. Liu, and D. Golberg, Nanotechnology **17**, 3648 (2006).
[10] E. W. Wong, P. E. Sheenhan, and C. M. Lieber, Science **277**, 1971 (1997).
[11] S. J. A. Koh, H. P. Lee, C. Lu, and Q. H. Cheng, Phys. Rev. B **72**, 085414 (2005).
[12] H. S. Park and J. A. Zimmerman, Phys. Rev. B **72**, 054106 (2005).
[13] E. Z. da Silva, F. D. Novaes, A. J. R. da Silva, and A. Fazzio, Phys. Rev. B **69**, 115411 (2004).
[14] H. S. Park, K. Gall, and J. A. Zimmerman, J. Mech. Phys. Solids **54**, 1862 (2006).
[15] S. J. A. Koh and H. P. Lee, Nanotechnology **17**, 3451 (2006).
[16] H. S. Park, Nano Lett. **6**, 958 (2006).
[17] M. A. Makeev, D. Srivastava, and M. Menon, Phys. Rev. B **74**, 165303 (2006).
[18] T. Y. Kim, S. S. Han, and H. M. Lee, Mater. Trans. **45**, 1442 (2004).
[19] A. J. Kulkarni, M. Zhou, K. Sarasamak, and S. Limpijumnong, Phys. Rev. Lett. **97**, 105502 (2006).
[20] J. Tersoff, Phys. Rev. Lett. **56**, 632 (1986).
[21] J. Tersoff, Phys. Rev. B **39**, 5566 (1989).
[22] K. Nordlund, J. Keinonen, and T. Mattila, Phys. Rev. Lett. **77**, 699 (1996).
[23] R. Devanathan, T. Diaz de la Rubia, and W. J. Weber, J. Nucl. Mater. **253**, 47 (1998).
[24] F. Gao and W. J. Weber, Phys. Rev. B **63**, 054101 (2000).
[25] Yu. N. Osetsky and A. Serra, Phys. Rev. B **57**, 755 (1998).
[26] P. Vashishta, R. K. Kalia, A. Nakano, and J. P. Rino, J. Appl. Phys. **101**, 103515 (2007).
[27] V. I. Ivashchenko, P. E. A. Turchi, and V. I. Shevchenko, Phys. Rev. B **75**, 085209 (2007).
[28] F. Gao and W. J. Weber, Appl. Phys. Lett. **82**, 913 (2003).
[29] F. Gao and W. J. Weber, Phys. Rev. B **66**, 024106 (2002).
[30] R. Devanathan, W. J. Weber, and F. Gao, J. Appl. Phys. **90**, 2303 (2001).
[31] L. J. Porter, J. Li, and S. Yip, J. Nucl. Mater. **246**, 53 (1997).
[32] M. J. Tang and S. Yip, Phys. Rev. B **52**, 15150 (1995).
[33] X. Luo, G. F. Qian, W. D. Fei, E. G. Wang, and C. F. Chen, Phys. Rev. B **57**, 9234 (1998).
[34] M. J. Tang and S. Yip, J. Appl. Phys. **76**, 2719 (1994).
[35] G. Z. Cambaz, G. N. Yushin, Y. Gogotsi, and V. G. Lutsenko, Nano Lett. **6**, 548 (2006).
[36] B. Wenzien, P. Käckell, and F. Bechstedt, Surf. Sci. **307-309**, 989 (1994).
[37] M. Sabisch, P. Krüger, and J. Pollmann, Phys. Rev. B **51**, 13367 (1995).
[38] W. R. L. Lambrecht, B. Segall, M. Methfessel, and M. van Schilfgaarde, Phys. Rev. B **44**, 3685 (1991).
[39] W. X. Li and T. Wang, Phys. Rev. B **59**, 3993 (1999).
[40] J. J. Petrovic, J. V. Milewski, D. L. Rohr, and F. D. Gac, J. Mater. Sci. **20**, 1167 (1985).
[41] T. Y. Kim, S. S. Han, and H. M. Lee, Mater. Trans. **45**, 1442 (2004).
[42] R. Stevens, J. Mater. Sci. **5**, 474 (1970).
[43] P. K. Sitch, R. Jones, S. Oberg, and M. I. Heggie, Phys. Rev. B **52**, 4951 (1995).
[44] S. P. Timoshenko and J. M. Gere, *Theory of Elastic Stability*, 2nd ed. (McGraw-Hill, New York, 1961), p. 541.
[45] S. C. Hung, Y. K. Su, T. H. Fang, S. J. Chang, and L. W. Ji, Nanotechnology **16**, 2203 (2005).